

Eccentricity estimation from initial data for Numerical Relativity Simulations

Alessandro Ciarfella,¹ James Healy,¹ Carlos O. Lousto,¹ and Hiroyuki Nakano²

¹*Center for Computational Relativity and Gravitation,
School of Mathematical Sciences, Rochester Institute of Technology,
85 Lomb Memorial Drive, Rochester, New York 14623, USA*

²*Faculty of Law, Ryukoku University, Kyoto 612-8577, Japan*

(Dated: June 29, 2022)

We describe and study an instantaneous definition of eccentricity to be applied at the initial moment of full numerical simulations of binary black holes. The method consists of evaluating the eccentricity at the moment of maximum separation of the binary. We estimate it using up to third post-Newtonian (3PN) order, and compare these results with those of evolving (conservative) 3PN equations of motion for a full orbit and compute the eccentricity e_r from the radial turning points, finding excellent agreement. We next include terms with spins up to 3.5PN, and then compare this method with the corresponding estimates of the eccentricity e_r^{NR} during full numerical evolutions of spinning binary black holes, characterized invariantly by a fractional factor $0 \leq f \leq 1$ of the initial tangential momenta. It is found that our initial instantaneous definition is a very useful tool to predict and characterize even highly eccentric full numerical simulations.

PACS numbers: 04.25.dg, 04.25.Nx, 04.30.Db, 04.70.Bw

I. INTRODUCTION

The concept of eccentricity is uniquely defined in Newtonian gravity. An extension to General Relativity is not strictly uniquely or even well defined, but we have found it useful to have a relationship to estimate an instantaneous eccentricity, e , defined at initial data.

To compute the numerical initial data, we use the puncture approach [1] along with the TWOPUNCTURES [2] code. For each eccentric family of simulations, we first determine the initial separation, R_c , and tangential quasicircular momentum, P_c using the results of [3]. To increase the eccentricity of the system while keeping the initial data at an apocenter, the initial tangential momentum, P_t , is modified by a fractional parameter, $0 \leq f \leq 1$, such that $P_t = (1 - f)P_c$. See Fig. 1 for an schematic representation.

This method was applied to the estimates of templates of the LIGO-Virgo detection GW190521 [4] in Ref. [5] and of the 824 simulations included in the latest (4th release [6]) RIT catalog of binary black hole simulations. In Refs. [5] and [6], the initial eccentricity was then approximately evaluated by the Newtonian relationship $e = 2f - f^2$. In this paper, we extend this definition to higher post-Newtonian (PN) orders to improve the identification of highly eccentric simulations and test it against full numerical evolutions.

II. METHOD

The idea of this method applied to PN expansions is to evaluate the conserved Hamiltonian at the two radial turning points of a binary, r_{\pm} , to evaluate j , the conserved angular momentum at those points and relate the eccentric and circular values at the apastron, r_+ , by a factor $(1 - f)$ as displayed in Fig. 1, for the full numeri-

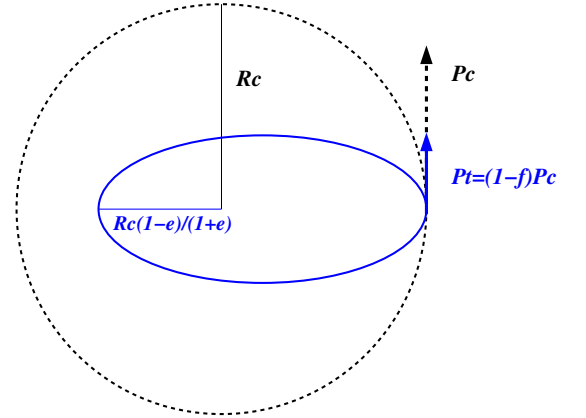


FIG. 1. Schematic of the initial momentum choice to describe eccentric orbits in Numerical Relativity. R_c and P_c denote the initial separation and tangential momentum for a quasicircular binary. Then, $P_t = (1 - f)P_c$ where f is a fractional parameter, $0 < f < 1$, is the initial tangential momentum for an eccentric binary with an instantaneous eccentricity, e .

cal case.

A. Nonspinning case

Let us begin with the nonspinning case, for which we can write the reduced Hamiltonian $\mathcal{H} = H/\mu$ with $\mu = m_1 m_2 / (m_1 + m_2)$,

$$\mathcal{H}(\mathbf{r}, \hat{\mathbf{p}}) = \mathcal{H}_0(\mathbf{r}, \hat{\mathbf{p}}) + \frac{1}{c^2} \mathcal{H}_1(\mathbf{r}, \hat{\mathbf{p}}) + \frac{1}{c^4} \mathcal{H}_2(\mathbf{r}, \hat{\mathbf{p}}) + \frac{1}{c^6} \mathcal{H}_3(\mathbf{r}, \hat{\mathbf{p}}), \quad (1)$$

where explicit expressions for the reduced 3PN Hamiltonian are given in Ref. [7] (see also Appendix A) with

$\mathbf{r} = \mathbf{R}/(GM)$ and $\hat{\mathbf{p}} = \mathbf{P}/\mu$ where \mathbf{R} is the relative separation vector, $M = m_1 + m_2$, and \mathbf{P} is the linear momentum. Writing this Hamiltonian in polar coordinates, we see that it does not depend on the coordinate ϕ , and so \hat{p}_ϕ is a conserved quantity and the motion will happen only on a plane and so $\hat{\mathbf{p}} = (\hat{p}_r, \hat{p}_\phi/r, 0)$. Now \hat{p}_r vanishes at the turning points r_+ and r_- , and we can write

$$\mathcal{H}(\mathbf{r}_\pm, \hat{\mathbf{p}}) = \mathcal{H}(r_\pm, \hat{p}_\phi) = \mathcal{H}(r_\pm, j), \quad (2)$$

where $j = \hat{p}_\phi$ is constant along the orbit.

We now define the eccentricity measure e_r as

$$e_r = \frac{r_+ - r_-}{r_+ + r_-}. \quad (3)$$

Therefore, r_- is given by

$$r_- = r_+ \frac{1 - e_r}{1 + e_r}, \quad (4)$$

(see Fig. 1).

To simplify more the computation, we scale again the Hamiltonian, the momentum, $\hat{\mathbf{p}}$, and the r -coordinate as

$$\tilde{\mathcal{H}} = r_+ \mathcal{H}, \quad \tilde{\mathbf{p}} = \sqrt{r_+} \hat{\mathbf{p}}, \quad \tilde{\mathbf{r}} = \frac{\mathbf{r}}{r_+}. \quad (5)$$

This allows us to rewrite the Hamiltonian as

$$\tilde{\mathcal{H}}(\tilde{\mathbf{r}}, \tilde{\mathbf{p}}) = \tilde{\mathcal{H}}_0(\tilde{\mathbf{r}}, \tilde{\mathbf{p}}) + \alpha \tilde{\mathcal{H}}_1(\tilde{\mathbf{r}}, \tilde{\mathbf{p}}) + \alpha^2 \tilde{\mathcal{H}}_2(\tilde{\mathbf{r}}, \tilde{\mathbf{p}}) + \alpha^3 \tilde{\mathcal{H}}_3(\tilde{\mathbf{r}}, \tilde{\mathbf{p}}), \quad (6)$$

where $\alpha = 1/(c^2 r_+)$.

The advantage of this rescaling is that in this way we explicitly remove the value of r_+ from our problem. This appears only in the expression for α . In particular, we have (in polar coordinates)

$$\tilde{r}_+ = 1, \quad \tilde{r}_- = \frac{1 - e_r}{1 + e_r}. \quad (7)$$

Now since the Hamiltonian is conserved along the orbit, we must have

$$\tilde{\mathcal{H}}(\tilde{r}_+, \tilde{j}) - \tilde{\mathcal{H}}(\tilde{r}_-, \tilde{j}) = 0, \quad (8)$$

where

$$\tilde{j} = \frac{j}{\sqrt{r_+}}. \quad (9)$$

Using Eq. (7), Eq. (8), and specifying values for α and η , we have an expression for \tilde{j} in terms of e_r . Finally, introducing a momentum suppression factor f as

$$\tilde{j}(e_r) = (1 - f) \tilde{j}_C, \quad (10)$$

where $\tilde{j}(0) = \tilde{j}_C$ for the circular orbit, we obtain

$$f(e_r) = 1 - \frac{\tilde{j}(e_r)}{\tilde{j}_C}. \quad (11)$$

This final expression provides us with the desired relationship to evaluate $f(e_r)$ and to invert (numerically) for any specific set of initial parameters of a binary black hole simulation and obtain the estimated e_r .

B. Spinning case

For the spinning case, we can apply the same method. Let us consider two orbiting, nonprecessing, black holes with spins \mathbf{S}_1 and \mathbf{S}_2 in the direction of the orbital angular momentum. The Hamiltonian becomes [8, 9] (we restore here the explicit dependence with the speed of light c to better display PN orders),

$$\begin{aligned} \mathcal{H}(\mathbf{r}, \mathbf{p}, \mathbf{S}_1, \mathbf{S}_2) = & \mathcal{H}_0(\mathbf{r}, \mathbf{p}) + \frac{1}{c^2} \mathcal{H}_1(\mathbf{r}, \mathbf{p}) + \frac{1}{c^4} \mathcal{H}_2(\mathbf{r}, \mathbf{p}) + \frac{1}{c^6} \mathcal{H}_3(\mathbf{r}, \mathbf{p}) \\ & + \frac{\delta}{c^2} \mathcal{H}_{SO}^{LO}(\mathbf{r}, \mathbf{p}, \mathbf{S}_1, \mathbf{S}_2) + \frac{\delta}{c^4} \mathcal{H}_{SO}^{NLO}(\mathbf{r}, \mathbf{p}, \mathbf{S}_1, \mathbf{S}_2) \\ & + \frac{\delta^2}{c^2} \mathcal{H}_{S1S2}^{LO}(\mathbf{r}, \mathbf{p}, \mathbf{S}_1, \mathbf{S}_2) + \frac{\delta^2}{c^2} \mathcal{H}_{S^2}^{LO}(\mathbf{r}, \mathbf{p}, \mathbf{S}_1, \mathbf{S}_2) \\ & + \frac{\delta^2}{c^4} \mathcal{H}_{S1S2}^{NLO}(\mathbf{r}, \mathbf{p}, \mathbf{S}_1, \mathbf{S}_2) + \frac{\delta^2}{c^4} \mathcal{H}_{S^2}^{NLO}(\mathbf{r}, \mathbf{p}, \mathbf{S}_1, \mathbf{S}_2) \\ & + \frac{\delta}{c^6} \mathcal{H}_{SO}^{NNLO}(\mathbf{r}, \mathbf{p}, \mathbf{S}_1, \mathbf{S}_2) + \frac{\delta^3}{c^4} \mathcal{H}_{S^3}^{LO}(\mathbf{r}, \mathbf{p}, \mathbf{S}_1, \mathbf{S}_2). \end{aligned} \quad (12)$$

where δ is a dimensionless factor that keeps track of the spin order of the term considered (see also Appendix A). In this case, we define

$$\tilde{\mathbf{S}}_a = \frac{\mathbf{S}_a}{\sqrt{r_+}} = \sqrt{\alpha} \boldsymbol{\chi}_a, \quad (a = 1, 2), \quad (13)$$

where in the last equality we introduced the dimensionless quantity $\boldsymbol{\chi}_a$ as

$$\boldsymbol{\chi}_a = \frac{\hat{\mathbf{S}}_a}{m_a^2}, \quad (a = 1, 2). \quad (14)$$

Here, $\hat{\mathbf{S}}_a$ are the actual spins with dimension (geometric units) $[\hat{\mathbf{S}}] = [(\text{Mass})]^2$. In terms of this new dimensionless variable we have the rescaled Hamiltonian as

$$\begin{aligned} \tilde{\mathcal{H}}(\tilde{\mathbf{r}}, \tilde{\mathbf{p}}, \boldsymbol{\chi}_1, \boldsymbol{\chi}_2) = & \tilde{\mathcal{H}}_0(\tilde{\mathbf{r}}, \tilde{\mathbf{p}}) + \alpha \tilde{\mathcal{H}}_1(\tilde{\mathbf{r}}, \tilde{\mathbf{p}}) + \alpha^2 \tilde{\mathcal{H}}_2(\tilde{\mathbf{r}}, \tilde{\mathbf{p}}) + \alpha^3 \tilde{\mathcal{H}}_3(\tilde{\mathbf{r}}, \tilde{\mathbf{p}}) \\ & + \alpha^{3/2} \tilde{\mathcal{H}}_{SO}^{LO}(\tilde{\mathbf{r}}, \tilde{\mathbf{p}}, \boldsymbol{\chi}_1, \boldsymbol{\chi}_2) + \alpha^{5/2} \tilde{\mathcal{H}}_{SO}^{NLO}(\tilde{\mathbf{r}}, \tilde{\mathbf{p}}, \boldsymbol{\chi}_1, \boldsymbol{\chi}_2) \\ & + \alpha^2 \tilde{\mathcal{H}}_{S1S2}^{LO}(\tilde{\mathbf{r}}, \tilde{\mathbf{p}}, \boldsymbol{\chi}_1, \boldsymbol{\chi}_2) + \alpha^2 \tilde{\mathcal{H}}_{S^2}^{LO}(\tilde{\mathbf{r}}, \tilde{\mathbf{p}}, \boldsymbol{\chi}_1, \boldsymbol{\chi}_2) \\ & + \alpha^3 \tilde{\mathcal{H}}_{S1S2}^{NLO}(\tilde{\mathbf{r}}, \tilde{\mathbf{p}}, \boldsymbol{\chi}_1, \boldsymbol{\chi}_2) + \alpha^3 \tilde{\mathcal{H}}_{S^2}^{NLO}(\tilde{\mathbf{r}}, \tilde{\mathbf{p}}, \boldsymbol{\chi}_1, \boldsymbol{\chi}_2) \\ & + \alpha^{7/2} \tilde{\mathcal{H}}_{SO}^{NNLO}(\tilde{\mathbf{r}}, \tilde{\mathbf{p}}, \boldsymbol{\chi}_1, \boldsymbol{\chi}_2) + \alpha^{7/2} \tilde{\mathcal{H}}_{S^3}^{LO}(\tilde{\mathbf{r}}, \tilde{\mathbf{p}}, \boldsymbol{\chi}_1, \boldsymbol{\chi}_2). \end{aligned} \quad (15)$$

We can now follow the same steps as indicated in Eqs. (8)–(11) to obtain a relationship between the fractional parameter f by which the tangential circular momentum is suppressed to generate eccentric orbits, and the eccentricity e_r , defined through the periastron and apastron (see also Appendix C).

III. RESULTS

In the applications below, we will assume for the sake of definiteness and comparisons with the simulations used for GW190521 in Ref. [5] an initial coordinate separation of the holes of about $r \approx 24.7M$, that we will use in the evaluation of α above. This corresponds in the cases studied in Ref. [5] to an initial quasircular reference frequency of 10 Hz for a $30 M_\odot$ system, as evaluated by the techniques described in Ref. [3].

A. Fractional parameter $f(e_r)$ for given initial parameters

The result for nonspinning equal mass binaries, i.e., the mass ratio $q = m_2/m_1 = 1$, at different successive PN orders is shown in Fig. 2. We plot here the factor f by which we reduce the tangential linear momentum of a quasircular orbit versus the computed eccentricity e_r . This allow us to read off the eccentricity associated to our initial data set up. We can see the good agreement to all displayed PN orders at low eccentricities ($e_r < 0.4$). At intermediate eccentricities the 1PN computation deviates from the higher order trend for $e_r > 0.4$, while the 2PN computation remains consistent for $e_r < 0.7$. The 3PN computation on the other hand converges towards the Newtonian (0PN) curve for larger e_r . We interpret this as the correct behavior since for large e_r the expected evolution of a binary is essentially a plunge that tends to reduce the differences between PN orders.

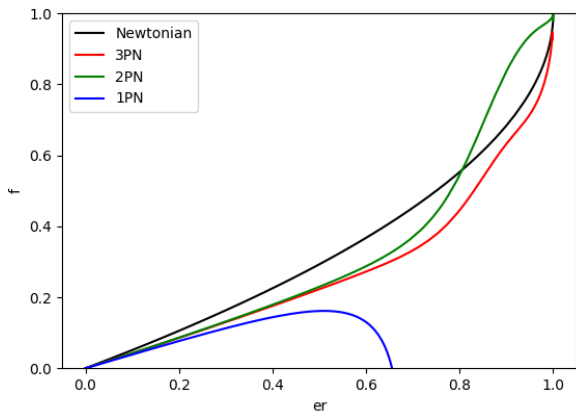


FIG. 2. Momentum suppression factor f vs. eccentricity e_r for nonspinning equal mass binaries, $\chi_i = 0$ and $q = 1$, at various PN orders.

In the case of spinning holes, we will hence focus directly on the 3PN computation and compare them with the nonspinning case. To better display the effects (and following comparisons with full numerics), we will consider the cases when both equal mass black holes have spins aligned ($\chi_i = +0.8$) or anti-aligned ($\chi_i = -0.8$)

with the orbital angular momentum (we checked that the $\chi_1 = -\chi_2$ case gives a curve very close to the nonspinning case). The results for this 3PN order comparisons for the various values of the spins are shown in Fig. 3. We observe a close dependence of the three curves for small and intermediate eccentricities, but for $e_r > 0.75$ there is a reverse in their relative behavior. While the case of aligned spins eventually merger for large eccentricities (plunges) with the nonspinning holes, the antialigned spins case shows a very different behavior. We will come back later to this case with a 3.5PN computation.

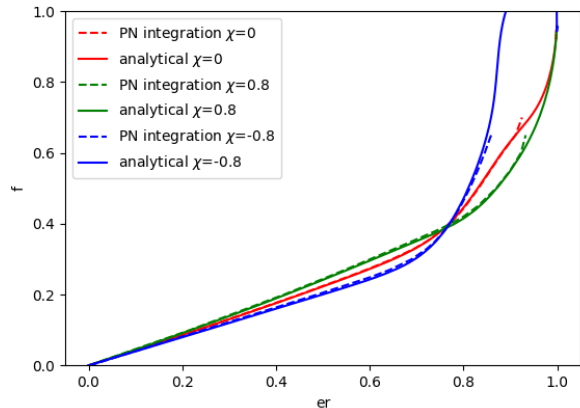


FIG. 3. Comparison of initial analytic vs. integration of the 3PN equations of motion: Eccentricity e_r vs. momentum suppression factor f for $q = 1$ and different values of the spins.

B. Comparison with numerical integrations of 3PN equations of motion

A first validation of our initial instantaneous eccentricity estimate can be performed by comparing our analytical results with the numerical integrations of the conservative 3PN equation of motion [10, 11], where we suppressed the 2.5PN radiative terms. We integrate the orbital motion over the first orbit and evaluate the eccentricity from the apastron and periastron differences, $e_r = (r_+ - r_-)/(r_+ + r_-)$. The comparisons for spinning and nonspinning cases with $q = 1$, and $\chi_i = 0, \pm 0.8$ are displayed in Fig. 3. The results show a notable agreement and consistency between the integrated and initial estimates of the eccentricity, for $e_r \leq 0.9$, at 3PN order.

To verify the mass ratio dependence of our eccentricity estimator as well, we compare our analytical results with numerical evolutions of the 3PN equations of motion in Fig. 4 for mass ratios $q = 1, 1/2$ and $1/3$ (for nonspinning binaries). We observe again a notable agreement in their corresponding regions or validity (as the 3PN approximation reduces its validity to medium and small eccentricity as we deal with smaller mass ratios).

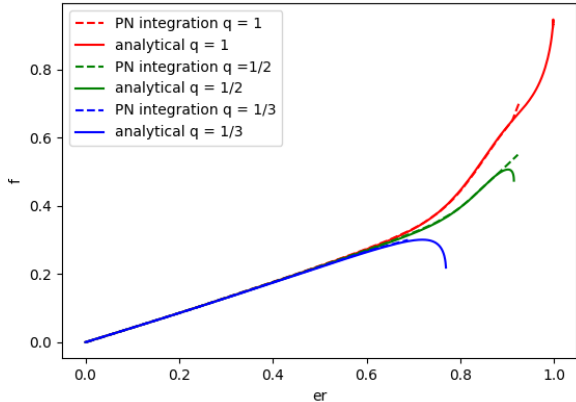


FIG. 4. Comparison of initial analytic vs. 3PN equation of motion integration of the momentum suppression factor f vs. eccentricity e_r for nonspinning binaries, $\chi_i = 0$ and different values of the mass ratio q .

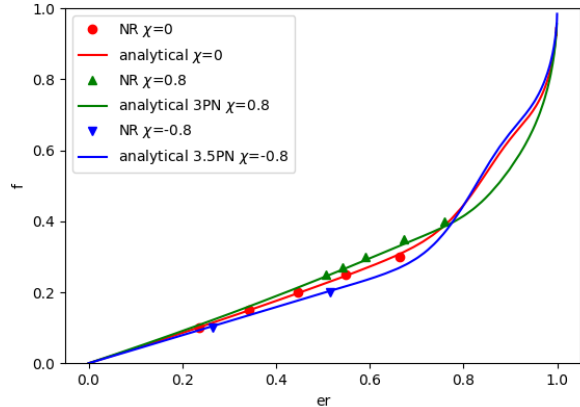


FIG. 5. Momentum suppression factor f vs. eccentricity e_r with PN estimates for various spins (continuous curves) in comparison with the full numerical simulation measurements (dots).

TABLE I. Eccentric simulations used in Fig. 5 and their estimated eccentricities from its radial turning points, e_r^{NR}

| RIT Catalog No. | R_c | q | χ_1^z | χ_2^z | f | e_r^{NR} |
|-----------------|-------|-----|------------|------------|------|------------|
| RIT:eBBH:1282 | 24.64 | 1 | 0.0 | 0.0 | 0.10 | 0.2357 |
| RIT:eBBH:1283 | 24.64 | 1 | 0.0 | 0.0 | 0.15 | 0.3416 |
| RIT:eBBH:1285 | 24.64 | 1 | 0.0 | 0.0 | 0.20 | 0.4459 |
| RIT:eBBH:1293 | 24.64 | 1 | 0.0 | 0.0 | 0.25 | 0.5488 |
| RIT:eBBH:1303 | 24.64 | 1 | 0.0 | 0.0 | 0.30 | 0.6646 |
| RIT:eBBH:1807 | 24.56 | 1 | 0.8 | 0.8 | 0.25 | 0.5064 |
| RIT:eBBH:1808 | 24.56 | 1 | 0.8 | 0.8 | 0.27 | 0.5410 |
| RIT:eBBH:1809 | 24.56 | 1 | 0.8 | 0.8 | 0.30 | 0.5915 |
| RIT:eBBH:1811 | 24.56 | 1 | 0.8 | 0.8 | 0.35 | 0.6735 |
| RIT:eBBH:1813 | 24.56 | 1 | 0.8 | 0.8 | 0.40 | 0.7587 |
| RIT:eBBH:1763 | 24.75 | 1 | -0.8 | -0.8 | 0.10 | 0.2644 |
| RIT:eBBH:1764 | 24.75 | 1 | -0.8 | -0.8 | 0.20 | 0.5143 |

C. Comparisons with full Numerical Relativity simulations

We are now able to directly compare our initial eccentricity PN estimates to actual full numerical simulations where it is possible to evaluate the eccentricity via the turning points in the simulations. We thus identify the numerical and PN (in ADMTT gauge) parameters, $R_c = r_+$ and $P_c = P_\phi(e_r = 0)/r_+$, and the values of f , α , q , and S_1 and S_2 for several simulations available in the RIT waveforms catalog [6] identified in Table I. The results are displayed in Fig. 5. The agreement for simulations in the range of low to middle eccentricities is remarkable. We also include here the 3.5PN corrections to the antialigned spins configurations to display an improved behavior all the way up to $e_r \rightarrow 1$, merging with the plunging behavior in the cases of nonspinning and aligned spins.

In the RIT catalog [6], we have another family of eccentric simulations (for nonspinning and different mass

ratios $q = 1, 3/4, 1/2$ and $1/4$), starting at much closer initial separations, $r \approx 11.35M$, that we can use to compare to our PN eccentric estimations. These separations are roughly half the ones we considered so far, and are at the limit of applicability of PN expansions. The results of these estimates are displayed in Fig. 6. It is also difficult to compute the e_r from the full numerical evolutions for large eccentricities since the trajectories are highly inspiral or merge before we can complete a meaningful orbit to extract r_+ and r_- . Yet, the estimates are very good for the expected range of validity of the PN expansions for small mass ratios (here $e_r < 0.5$).

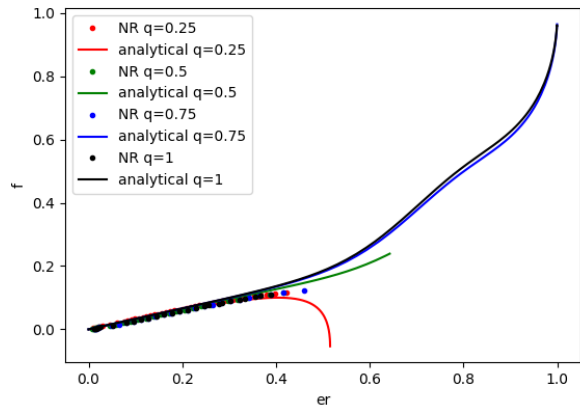


FIG. 6. Momentum suppression factor f vs. eccentricity e_r for various mass ratio nonspinning binaries using 3PN estimates (continuous curves) at $r = 11.35M$, in comparison with the corresponding full numerical simulations evaluations (dots).

We conclude that our eccentricity estimates provide an accurate description of the initial binary black holes

eccentric properties and can be directly applied to the eccentric simulations in the 4th RIT catalog [6].

IV. CONCLUSIONS AND DISCUSSION

We have defined eccentric binary black hole simulations invariantly in terms of fractional, $f = 1 - P_t(e_r)/P_c$, tangential linear momenta to the circular one. We have found that the PN analytic estimates of the initial eccentricity of these full numerical simulations are an accurate and practical tool to predict and assess the first orbit eccentricity of full numerical simulations, allowing, for instance, precise design of new runs for parameter coverage or targeted studies. For low and medium eccentricities $e_r < 0.5$, and separated enough binaries, even 2PN estimates are accurate. For higher eccentricities and highly spinning (particularly for both antialigned) binary black holes, we require 3PN, 3.5PN or even eventually 4PN estimates at closer initial separations. Our formalism can be also applied to generic orientations of the spins by use of the concept of spherical orbits [12] to compute the turning points r_{\pm} .

Here, we have suppressed the tangential momentum with respect to the quasicircular one by a $(1 - f)$ factor, with $0 \leq f \leq 1$. But if we allow for $f < 0$, we would actually increase the tangential momentum, leading to an elliptic orbit, but starting at the periastron (r_-) instead of the apastron (r_+). This can be achieved by reversing the sign of e in our equations. For instance, for the Newtonian case we would have $e_r = -2f + f^2$ for $F_p < f \leq 0$, where in this case $F_p = 1 - \sqrt{2} = -0.4142\dots$ would lead to a parabola. For values more negative than this F_p , i.e., $f < F_p$, we would generate a hyperbolic orbit.

The estimates which we have developed can now be directly applied to the 824 eccentric simulations in the 4th RIT catalog [6]. Our formulas should still provide good estimates for well separated precessing binaries with small radial momentum components by use of the projected spins along the initial orbital angular momentum as variables. This is the case for all our simulations in Ref. [6], and in particular we can now reassess the best eccentricity estimate of the gravitational waves event GW190521 [5]. In that paper, we assessed the eccentricity of the optimal full numerical simulation with the Newtonian estimate to be $e_N = 0.69$ (with $q = 1$, $\chi_1^z = \chi_2^z = 0.27$, $R_c = 24.7M$, and $f = 0.44$). We can now recompute the eccentricity using our 3.5PN estimator and find $e_{PN} = 0.80$, which highlights again the potentially interesting astrophysical scenarios that might have lead to the merger of the two black holes generating GW190521 [13, 14].

ACKNOWLEDGMENTS

The authors gratefully acknowledge the National Science Foundation (NSF) for financial support from Grant

No. PHY-1912632. Computational resources were also provided by the NewHorizons, BlueSky Clusters, GreenPrairies, and WhiteLagoon at the Rochester Institute of Technology, which were supported by NSF grants No. PH-0722703, No. DMS-0820923, No. AST-1028087, No. PHY-1229173, No. PH-1726215, and No. PH-2018420. This work used the Extreme Science and Engineering Discovery Environment (XSEDE) [allocation TG-PHY060027N], which is supported by NSF grant No. ACI-1548562 and project PHY20007 Frontera, an NSF-funded petascale computing system at the Texas Advanced Computing Center (TACC). H.N. is supported by JSPS/MEXT KAKENHI Grant No. JP21K03582, No. JP21H01082, and No. JP17H06358.

Appendix A: PN Hamiltonian

In this appendix we provide the explicit form of the Hamiltonian terms (up to 2PN order) that we used throughout this paper. From Eq. (7) in Ref. [7], we have the nonspinning components of the Hamiltonian,

$$\mathcal{H}_0(\mathbf{r}, \hat{\mathbf{p}}) = \frac{\hat{\mathbf{p}}^2}{2} - \frac{1}{r}, \quad (\text{A1})$$

$$\begin{aligned} \mathcal{H}_1(\mathbf{r}, \mathbf{p}) = & \frac{1}{8}(3\eta - 1)(\hat{\mathbf{p}}^2)^2 - \frac{1}{2r} [(3 + \eta)\hat{\mathbf{p}}^2 + \eta(\mathbf{n} \cdot \hat{\mathbf{p}})^2] \\ & + \frac{1}{2r^2}, \end{aligned} \quad (\text{A2})$$

$$\begin{aligned} \mathcal{H}_2(\mathbf{r}, \mathbf{p}) = & \frac{1}{16}(1 - 5\eta + 5\eta^2)(\hat{\mathbf{p}}^2)^3 \\ & + \frac{1}{8r} [(5 - 20\eta - 3\eta^2)(\hat{\mathbf{p}}^2)^2 - 2\eta^2(\mathbf{n} \cdot \hat{\mathbf{p}})^2\hat{\mathbf{p}}^2 - 3\eta^2(\mathbf{n} \cdot \hat{\mathbf{p}})^4] \\ & + \frac{1}{2r^2} [(5 + 8\eta)\hat{\mathbf{p}}^2 + 3\eta(\mathbf{n} \cdot \hat{\mathbf{p}})^2] - \frac{1}{4r^3}(1 + 3\eta), \end{aligned} \quad (\text{A3})$$

where $\eta = m_1 m_2 / (m_1 + m_2)^2$.

The explicit expressions for the spin terms of the Hamiltonian are given in Eqs. (13)–(16) of Ref. [8] and Eqs. (15)–(18) of Ref. [9]. Here we write some of them in the notation used throughout this paper

$$\begin{aligned} \mathcal{H}_{SO}^{LO}(\mathbf{r}, \mathbf{p}) = & \frac{1}{r^3} \left[\left(1 - \frac{\eta}{2} + \sqrt{1 - 4\eta} \right) (\mathbf{h} \cdot \mathbf{S}_1) \right. \\ & \left. + \left(1 - \frac{\eta}{2} - \sqrt{1 - 4\eta} \right) (\mathbf{h} \cdot \mathbf{S}_2) \right], \end{aligned} \quad (\text{A4})$$

$$\begin{aligned} \mathcal{H}_{S^2}^{LO}(\mathbf{r}, \mathbf{p}) = & \frac{\eta}{r^3} \left[\lambda_1 \left(-1 + 2\eta - \sqrt{1 - 4\eta} \right) \left(3(\mathbf{n}_{12} \cdot \mathbf{S}_1)^2 - (\mathbf{S}_1 \cdot \mathbf{S}_1) \right) \right. \\ & \left. + \lambda_2 \left(-1 + 2\eta + \sqrt{1 - 4\eta} \right) \left(3(\mathbf{n}_{12} \cdot \mathbf{S}_2)^2 - (\mathbf{S}_2 \cdot \mathbf{S}_2) \right) \right], \end{aligned} \quad (\text{A5})$$

$$\mathcal{H}_{S_1 S_2}^{LO}(\mathbf{r}, \mathbf{p}) = \frac{\eta}{r^3} (3(\mathbf{n}_{12} \cdot \mathbf{S}_1)(\mathbf{n}_{12} \cdot \mathbf{S}_2) - (\mathbf{S}_1 \cdot \mathbf{S}_2)), \quad (\text{A6})$$

where for BHs $\lambda_1 = \lambda_2 = -1/2$, $\mathbf{n}_{12} = \mathbf{r}/|r|$ and $\mathbf{h} = r\mathbf{n}_{12} \times \hat{\mathbf{p}}$.

Appendix B: Scripts/Notebooks

Here, we present a minimalistic script to compute the eccentricity from the full numerical simulation parameters q , R , χ_1^z , χ_2^z and f . For the sake of simplicity we only include explicitly up to the 2PN Hamiltonian terms, but in the results of the paper we computed up to 3.5PN terms. The script only allows for spins oriented along the z axis but it can be extended in order to include any orientation of the spins. 4PN local terms can be added in a straightforward way too, but the non local (see Ref. [15]) terms are more difficult to include in our formalism.

Appendix C: Explicit analytic expressions for 1PN

Here, we derive explicit analytic expressions for $f(e_r)$ at a lower PN order expansions in the eccentricity, We

hence consider the 1PN Hamiltonian,

$$H = \frac{1}{2} \frac{P_\phi^2}{r^2} - \frac{1}{r} + \alpha \left[\frac{1}{8} \frac{(3\eta - 1) P_\phi^4}{r^4} - \frac{1}{2} \frac{(3 + \eta) P_\phi^2}{r^3} + \frac{1}{r^2} \right] \quad (\text{C1})$$

From equating the values of the Hamiltonian at the periastron and apastron, r_+ ,

$$H(r = r_+, P_\phi^2) = H(r = r_+(1 - e_r)/(1 + e_r), P_\phi^2), \quad (\text{C2})$$

picking up the right root of P_ϕ^2 , we find for our approximation of $f(e_r) = 1 - \sqrt{P_\phi^2/P_\phi^2(e_r = 0)}$

$$f(e_r) = - \frac{\left[-\Delta + \frac{\alpha(22-6\eta)-4}{\Delta} - 3\alpha(\eta+3) + 4 \right] e_r}{2(\Delta + 3\alpha(\eta+3) - 2)}, \quad (\text{C3})$$

where

$$\Delta = \sqrt{\alpha(\alpha(9\eta^2 + 30\eta + 89) + 12\eta - 44) + 4}. \quad (\text{C4})$$

This expression is formally valid for $e_r < 0.3$, but it can be used as a first estimate up to intermediate eccentricities, $e_r < 0.6$ in the large separation regime $r_+ > 12M$, comparable masses, $q > 1/4$, and slowly spinning black holes $\chi_i < 0.5$, as we verified by direct comparisons with full 3PN expressions.

-
- [1] S. Brandt and B. Brügmann, Phys. Rev. Lett. **78**, 3606 (1997), gr-qc/9703066.
 - [2] M. Ansorg, B. Brügmann, and W. Tichy, Phys. Rev. **D70**, 064011 (2004), gr-qc/0404056.
 - [3] J. Healy, C. O. Lousto, H. Nakano, and Y. Zlochower, Class. Quant. Grav. **34**, 145011 (2017), arXiv:1702.00872 [gr-qc].
 - [4] R. Abbott *et al.*, Phys. Rev. Lett. **125**, 101102 (2020).
 - [5] V. Gayathri, J. Healy, J. Lange, B. O'Brien, M. Szczepanczyk, I. Bartos, M. Campanelli, S. Klimentko, C. O. Lousto, and R. O'Shaughnessy, Nature Astron. **6**, 344 (2022), arXiv:2009.05461 [astro-ph.HE].
 - [6] J. Healy and C. O. Lousto, Phys. Rev. D **105**, 124010 (2022), arXiv:2202.00018 [gr-qc].
 - [7] R.-M. Memmesheimer, A. Gopakumar, and G. Schafer, Phys. Rev. D **70**, 104011 (2004), arXiv:gr-qc/0407049.
 - [8] M. Tessmer, J. Hartung, and G. Schafer, Class. Quant. Grav. **27**, 165005 (2010), arXiv:1003.2735 [gr-qc].
 - [9] M. Tessmer, J. Hartung, and G. Schafer, Class. Quant. Grav. **30**, 015007 (2013), arXiv:1207.6961 [gr-qc].
 - [10] T. Damour, P. Jaranowski, and G. Schafer, Phys. Rev. **D77**, 064032 (2008), arXiv:0711.1048 [gr-qc].
 - [11] A. Buonanno, Y. Chen, and T. Damour, Phys. Rev. **D74**, 104005 (2006), gr-qc/0508067.
 - [12] A. Buonanno, L. E. Kidder, A. H. Mroue, H. P. Pfeiffer, and A. Taracchini, Phys. Rev. **D83**, 104034 (2011), arXiv:1012.1549 [gr-qc].
 - [13] R. Abbott *et al.* (LIGO Scientific, Virgo), Astrophys. J. Lett. **900**, L13 (2020), arXiv:2009.01190 [astro-ph.HE].
 - [14] O. Barrera and I. Bartos, Astrophys. J. Lett. **929**, L1 (2022), arXiv:2201.09943 [astro-ph.HE].
 - [15] G. Schäfer and P. Jaranowski, Living Rev. Rel. **21**, 7 (2018), arXiv:1805.07240 [gr-qc].

```

::usr/local/bin/wolframscript

If[Length[ScriptCommandLine] < 6, Print["Not enough arguments.
The argument format
  is:\nmass_ratio GM/(rc^2) Spin_mass_1 Spin_mass_2 f "];
Quit[]]

H0 = P^2/2 - 1/r;
H1 = (3η-1)P^4/8 - 1/(2r)(3+η)P^2 + 1/(2r^2);
HSOLO = P/(r^2)((1-η/2 + Sqrt[1-4η])S1 + (1-η/2 - Sqrt[1-4η])S2);
H2 = (1-5η+5η^2)/16P^6 + 1/(8r)(5-20η-3η^2)P^4 +
  1/(2r^2)(5+8η)P^2 - 1/(4r^3)(1+3η);
HS1S2L0 = η/(r^3)(-S1S2);
HS2L0 =
  1/(2r^3)(-λ1(-1+2η-Sqrt[1-4η])S1S1 - λ2(-1+2η+Sqrt[1-4η])S2S2);
HSOHL0 = 0;
H3 = 0;
HS1S2NLO = 0;
HS2NLO = 0;
HSOHLNLO = 0;
HS3LO = 0;

Clear[Pphi, PphiC, f];

P = Pphi/r;

q = ToExpression[ScriptCommandLine[2]];
η = Rationalize[q/(1+q)^2];
α = Rationalize[ToExpression[ScriptCommandLine[3]]];
S1 = Rationalize[ToExpression[ScriptCommandLine[4]]];
S2 = Rationalize[ToExpression[ScriptCommandLine[5]]];
λ1 = -1/2;
λ2 = -1/2;
CQ1 = 1;
CQ2 = 1;

H = H0 + αH1 + α^2(3/2)HSOLO + α^2(HS1S2L0 + HS2L0 + H2) + α^2(5/2)(HSOHL0) +
  α^3(H3 + HS1S2NLO + HS2NLO) + α^3(7/2)(HSOHLNLO + HS3LO);

s = Solve[(D[H, r] r^5 /. r -> 1) == 0, Pphi];

```

```

PphiC = Select[
  Select[N[s[All, 1, 2]], Abs[Im[#]] < 10^-13 &], Re[#] ≥ 1 && Re[#] < 2 &][[1]]

ra = 1;
rp = (1-e)/(1+e);

Hp = (H /. r -> rp);
Ha = (H /. r -> ra);

s2 = Solve[(Ha - Hp)(1-e)^6/e == 0, Pphi];

Pphi = s2[Position[N[s2[All, 1, 2]] /. e -> 0],
  Select[Select[N[s2[All, 1, 2]] /. e -> 0],
    Abs[Im[#]] < 10^-13 &], Re[#] ≥ 1 && Re[#] < 2 &][[1]]][[1, 1], 1, 2];

N[Pphi /. e -> 0]

f = ToExpression[ScriptCommandLine[6]]

If[TimeConstrained[NSolve[1 - Pphi/PphiC = f, e][1, 1, 2], 20., 0] == 0 ||
  NSolve[1 - Pphi/PphiC = f, e] == {},
  Print["The f value inserted does not give a solution for the PNOrder chosen"],
  Print[NSolve[1 - Pphi/PphiC = f, e][1, 1, 2]]]

f = 1 - Pphi/PphiC;

```

FIG. 7. Script to evaluate the eccentricity (explicit to 2PN order).